THE JOURNAL OF BIOLOGICAL CHEMISTRY VOL. 291, NO. 52, pp. 26937–26949, December 23, 2016

Receptor MER Tyrosine Kinase Proto-oncogene (MERTK) Is Not Required for Transfer of Bis-retinoids to the Retinal Pigmented Epithelium*[S]

Received for publication, October 24, 2016, and in revised form, November 14, 2016 Published, JBC Papers in Press, November 14, 2016, DOI 10.1074/jbc.M116.764563

Grazyna Palczewska[‡1], Akiko Maeda[§1,2], Marcin Golczak[¶], Eisuke Arai[§], Zhiqian Dong[‡], Lindsay Perusek[§], Brian Kevany[¶], and Krzysztof Palczewski[¶3]

From [‡]Polgenix, Inc. and the Departments of [§]Ophthalmology and Visual Sciences and [¶]Pharmacology and Cleveland Center for Membrane and Structural Biology, School of Medicine, Case Western Reserve University, Cleveland, Ohio 44106

Edited by George Carman

Accumulation of bis-retinoids in the retinal pigmented epithelium (RPE) is a hallmark of aging and retinal disorders such as Stargardt disease and age-related macular degeneration. These aberrant fluorescent condensation products, including di-retinoid-pyridinium-ethanolamine (A2E), are thought to be transferred to RPE cells primarily through phagocytosis of the photoreceptor outer segments. However, we observed by two-photon microscopy that mouse retinas incapable of phagocytosis due to a deficiency of the c-Mer proto-oncogene tyrosine kinase (Mertk) nonetheless contained fluorescent retinoid condensation material in their RPE. Primary RPE cells from *Mertk*$^{-/-}$ mice also accumulated fluorescent products *in vitro*. Finally, quantification of A2E demonstrated the acquisition of retinal condensation products in *Mertk*$^{-/-}$ mouse RPE prior to retinal degeneration. In these mice, we identified activated microglial cells that likely were recruited to transport A2E-like condensation products to the RPE and dispose of the dying photoreceptor cells. These observations demonstrate a novel transport mechanism between photoreceptor cells and RPE that does not involve canonical Mertk-dependent phagocytosis.

Maintaining the health of the vertebrate retina requires a delicate interaction between retinal photoreceptor cells, which collect and transmit visual stimuli, and the adjacent retinal pigmented epithelium (RPE),[4] a cell layer that forms part of the blood-retina barrier (1). Disturbances in this interaction, whether through genetic defects, environmental insults, or trauma can lead to retinal degeneration and ultimate loss of vision (2, 3). The RPE performs many vital functions, including the daily removal of the older distal portions of photoreceptor outer segments (4–6) and the delivery of both nutrients and the 11-*cis*-retinal chromophore to rod and cone photoreceptor cells that sustain vision (7). Roughly 10% of each photoreceptor cell outer segment is shed daily throughout an animal's life, distinguishing the RPE as perhaps the most active phagocytic cell layer in the body (5). Although RPE phagocytosis was discovered over 40 years ago (4), the molecular mechanisms underlying this process have not been delineated. However, certain molecular components that support classic phagocytosis have been identified, including the tyrosine receptor kinase Mertk (8, 9). The RPE not only removes toxic photo-oxidation products that accumulate in the retina, but it also recycles usable materials such as proteins, lipids, and small molecules. Retinoid condensation products such as bis-retinoids (di-retinoid-pyridinium-ethanolamine (A2E), retinoid dimers, and others) generated in photoreceptors are presumably transported along with photoreceptor membranes to the RPE during phagocytosis. Highly fluorescent A2E accumulation is a pathogenic hallmark of Stargardt disease, the most common juvenile form of human macular degeneration (10). A2E accumulation also is thought to contribute to the pathogenesis of age-related macular degeneration (AMD) (11). Moreover, increased fluorescence in the RPE over time is used as a biomarker of progressive retinal disease (12, 13). Thus, elucidating the molecular mechanisms of formation and transport of these fluorophores is important both for understanding the cell biology of the retina as well as establishing potential diagnostic markers and devising therapeutic compounds for retinal diseases.

* This work was supported in part by National Institutes of Health Grants EY022326, U01 EY025451, and R24 EY024864 (to K. P.), EY022658 (to A. M.), and EY023948 (to M. G.), VSRC CORE Grant P30 EY011373, the Arnold and Mabel Beckman Foundation, and the Foundation Fighting Blindness. The authors declare that they have no conflicts of interest with the contents of this article. The content is solely the responsibility of the authors and does not necessarily represent the official views of the National Institutes of Health.

[S] This article contains supplemental Movies S1 and S2.

The processed and raw fastq files deposited in NCBI GEO database are GSE84932 for R. norvegicus and GSE84930 for H. sapiens.

[1] Both authors contributed equally to this work.

[2] Recipient of the 2014 RBP Sybil B. Harrington Catalyst Award. To whom correspondence may be addressed. Tel.: 216-368-0670; Fax: 216-368-3171; E-mail: aam19@case.edu.

[3] The John H. Hord Professor of Pharmacology. To whom correspondence may be addressed: Dept. of Pharmacology, School of Medicine, Case Western Reserve University, 10900 Euclid Ave., Cleveland, OH 44106. Tel.: 216-368-4631; Fax: 216-368-1300; E-mail: kxp65@case.edu.

[4] The abbreviations used are: RPE, retinal pigmented epithelium; A2E, di-retinoid-pyridinium-ethanolamine; AMD, age-related macular degeneration; MERTK, MER tyrosine kinase proto-oncogene; TPM, two-photon fluorescent excitation microscopy; RCS, Royal College of Surgeons; AdipoR, adiponectin receptor; BMM, bone marrow macrophage; DHA, docosahexaenoic acid; RPKM, reads per kilobase per million; PNA, peanut agglutinin; DKO, *Abca4*$^{-/-}$*Rdh8*$^{-/-}$; TKO, *Mertk*$^{-/-}$, and *Mertk*$^{-/-}$*Abca4*$^{-/-}$*Rdh8*$^{-/-}$.

Phagocytosis involves the transfer of membranous and soluble materials from the photoreceptors to the RPE. However, a reverse transport process also occurs whereby the RPE regenerates the visual chromophore, 11-*cis*-retinal, for final delivery to the photoreceptors (14, 15). Unfortunately, both phagocytosis and the reverse process are not easily investigated. Thus, we have been developing two-photon fluorescence microscopy (TPM) as a non-invasive approach to study the intact two-cell system composed of RPE and photoreceptor cells (16, 17). Here, we investigated the relationships between RPE phagocytosis, alternative mechanisms of retinoid recycling, and A2E accumulation *in vivo* by using a combination of genetically modified mouse models, imaging by TPM, and analytical methods. Surprisingly, we discovered that retinoid condensation products can be transferred to the RPE without classic Mertk-dependent phagocytosis, thereby identifying a novel mode of retinoid transfer within the eye.

Results

TPM and Retinoid Analysis Reveals Temporal Changes at the RPE-Photoreceptor Interface—Given the close proximity of photoreceptor outer segments to the RPE, special imaging techniques are needed to separate the individual contributions of these two cell types with respect to the normal processing of retinoids as well as to the generation of modified retinoid deposits associated with aging and certain retinal degenerative diseases. To overcome the obstacle of imaging these apposing cell types, we employed TPM to characterize temporal changes at the RPE-photoreceptor interface. Because emission of retinyl esters and condensation products largely overlaps in the retina, we performed a systematic analysis of fluorescence intensity ratios for excitation light at both 730 and 850 nm to differentiate primarily between retinyl esters and A2E-like condensation products.

Three-dimensional (3D) reconstructions of the RPE in 3-month-old wild-type (WT) mice confirmed the presence of organized retinosomes, lipid droplet-like structures containing retinyl esters that participate in the normal visual cycle (Fig. 1, *top panel*) (18). These findings were then compared with those obtained from $Mertk^{-/-}Abca4^{-/-}Rdh8^{-/-}$ mice. $Abca4^{-/-}Rdh8^{-/-}$ mice lack proteins critical for the clearance of all-*trans*-retinal from photoreceptors and manifest increased fluorescent products as well as a severe RPE-photoreceptor dystrophy reminiscent of Stargardt disease (17, 19). We examined these mice bred on a phagocytosis-deficient $Mertk^{-/-}$ background. In contrast to WT retinas, enlarged fluorescent granules were seen in both the RPE and photoreceptors of age-matched $Mertk^{-/-}Abca4^{-/-}Rdh8^{-/-}$ mice (Fig. 1, *bottom panel*). Enlarged fluorescent granules were visible with both 730 and 850 nm excitation light. This initial observation was intriguing because Mertk-dependent phagocytosis of photoreceptor outer segments was thought to be required for the accumulation of 850 nm excitable fluorophores in the RPE (20, 21).

TPM spectral analysis of the RPE in 3-month-old $Mertk^{-/-}Abca4^{-/-}Rdh8^{-/-}$ mice revealed two types of fluorescent deposits, namely those excited with 730 but not 850 nm light (Fig. 2*A*, *red arrows*) and deposits that responded to both 730 and 850 nm (Fig. 2*A*, *white arrows*). Deposits excited by 730 but not 850 nm excitation light had emission spectra characteristic of retinosomes that store all-*trans*-retinyl esters in the RPE (16, 18, 22) and differ from other portions of the RPE (Fig. 2*B*). To verify this finding, we performed an analysis of mouse eyes and detected accumulation of all-*trans*-retinyl esters in 3-month-old $Mertk^{-/-}$ mice (Fig. 2*C*). Low levels of 11-*cis*-retinal are indicative of severe photoreceptor degeneration in $Mertk^{-/-}Abca4^{-/-}Rdh8^{-/-}$ and $Mertk^{-/-}$ mice and greater accumulation of 11-*cis*-retinal precursor, all-*trans*-retinyl esters could be an early pathological sign of retinal degeneration associated with Mertk impairment. Vacuoles previously detected in the RPE of $Rpe65^{-/-}$ mice with elevated levels of all-*trans*-retinyl

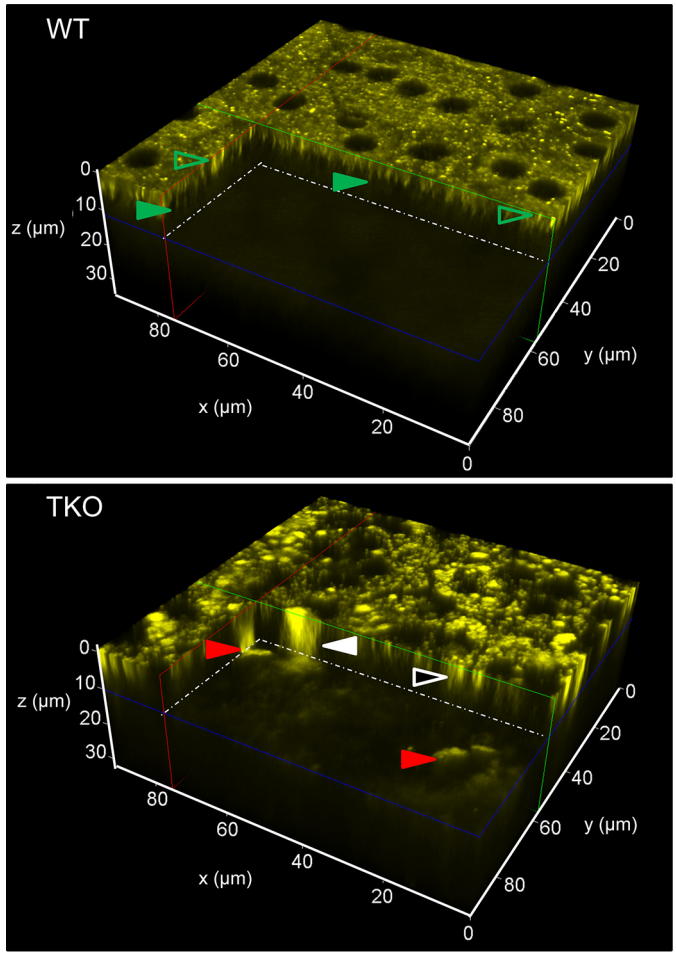

FIGURE 1. **Differences between WT and TKO mice in the distribution of fluorophores in the RPE and photoreceptor cells.** TPM 3D reconstructions of the RPE/retina interface in 3-month-old WT and $Mertk^{-/-}Abca4^{-/-}Rdh8^{-/-}$ (TKO) mice are shown. The center of the RPE was set at $z = 0$ μm with the photoreceptor space starting at 8 μm below. In TKO mice, *red arrowheads* point to large (over 20 μm) fluorescent granules that extend from $z \approx 6$ μm below the RPE cell layer (17). Fluorescent granules of this size, shape, and location that display an emission spectrum with a broad maximum at 600 nm were previously identified as infiltrating microglia/macrophages (17). Another type of large fluorescent granule is indicated with a *white arrowhead*. These granules extended throughout the thickness of the RPE and into the space below. Smaller granules in the RPE are indicated with a *white-outlined black arrowhead*. In WT mice, fluorescence in the photoreceptor space was faint and uniform. Most fluorescent structures in the RPE, indicated with *green outlined transparent arrowheads*, represent retinosomes (retinyl ester-containing lipid droplets) (18, 22) characterized by their 1-μm size and emission spectra with a broad maximum at 500 nm. Microvilli visible at about 5 μm below the center of RPE are indicated with *solid green arrowheads*.

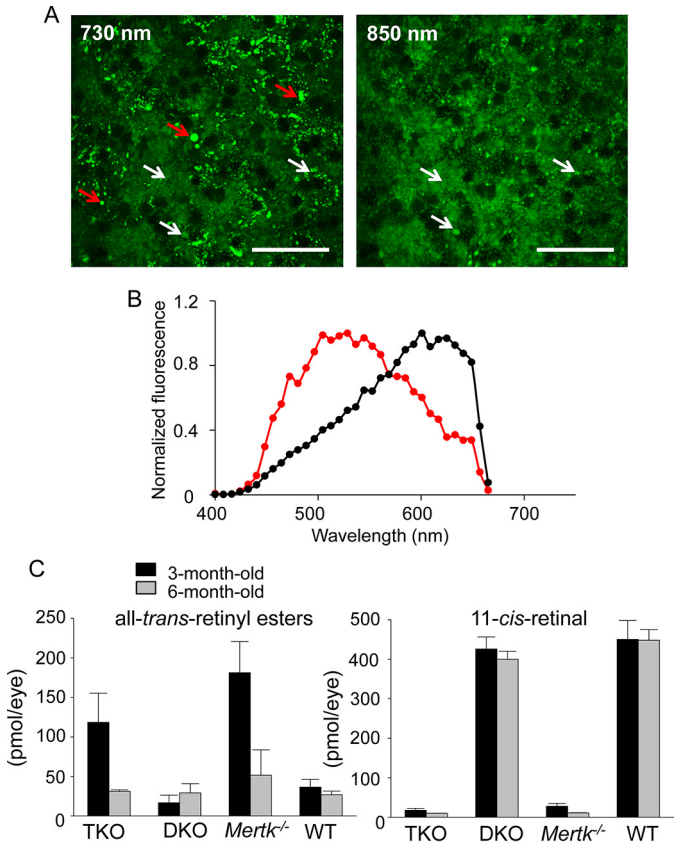

FIGURE 2. **Accumulation of all-*trans*-retinyl esters in the RPE.** Aberrant accumulation of all-*trans*-retinyl esters occurs during the process of retinal degeneration in *Mertk*$^{-/-}$ mice. *A,* TPM images of the RPE in a 3-month-old *Mertk*$^{-/-}$*Abca4*$^{-/-}$*Rdh8*$^{-/-}$ (TKO) mouse with excitation wavelengths shown. *Red arrows* indicate fluorescent deposits responding to λ_{ex} = 730 nm but not λ_{ex} = 850 nm light, and *white arrows* indicate fluorescent deposits that respond to both 730 and 850 nm light. *Scale bars,* 50 μm. *B,* TPM fluorescence emission spectra from the RPE obtained with λ_{ex} = 730 nm light. The spectrum from fluorescent deposits with λ_{ex} = 730 nm but not with λ_{ex} = 850 nm light stimulation is in *red*. An average spectrum from the RPE dominated by longer wavelength emitting fluorophores is shown in *black*. *C,* quantification of all-*trans*-retinyl esters and the visual chromophore and 11-*cis*-retinal by normal-phase HPLC is shown. *Bars* indicate S.D.s. $n \geq 3$ animals.

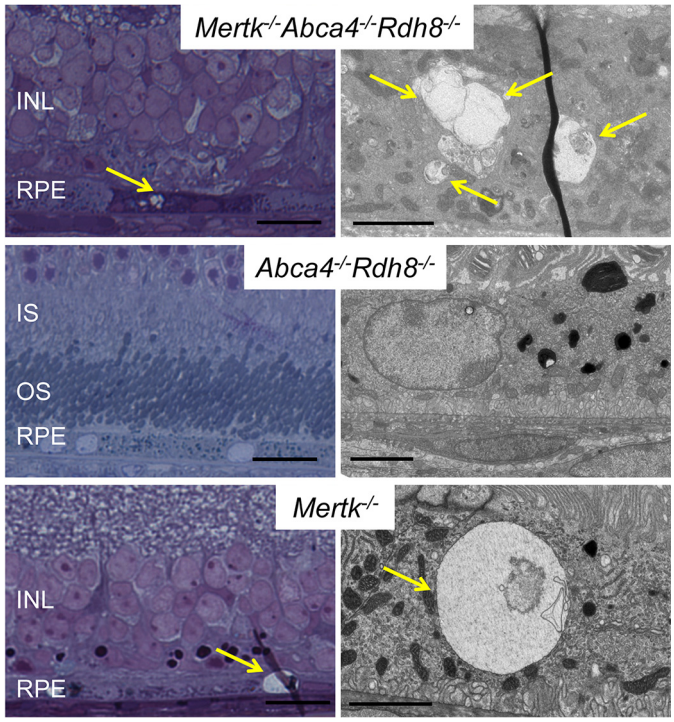

FIGURE 3. **RPE vacuoles in *Mertk*$^{-/-}$ and *Mertk*$^{-/-}$*Abca4*$^{-/-}$*Rdh8*$^{-/-}$ mice.** All-*trans*-retinyl esters accumulate in the RPE and form vacuoles as observed by EM. Representative toluidine blue-stained thick retinal Epon sections from 6-month-old *Mertk*$^{-/-}$*Abca4*$^{-/-}$*Rdh8*$^{-/-}$, *Abca4*$^{-/-}$*Rdh8*$^{-/-}$, and *Mertk*$^{-/-}$ mice are presented (*left panels*). *Right panels* show representative electron micrographs of RPE cells from these mice. *Yellow arrows* point to vacuoles in RPE cells. *Scale bars* in the *right* and *left panels* indicate 20 and 2 μm. *INL,* inner nuclear layer; *IS,* inner segment; *OS,* outer segment.

esters (23) were also observed in the RPE of mice with *Mertk* deficiency (Fig. 3).

Age-dependent Changes in Mertk-deficient Mice—As a consequence of the above findings, we analyzed the RPE in greater detail in 1- and 6-month-old mice among four genotypes as follows: WT; *Abca4*$^{-/-}$*Rdh8*$^{-/-}$; *Mertk*$^{-/-}$; and *Mertk*$^{-/-}$*Abca4*$^{-/-}$*Rdh8*$^{-/-}$. At 1 month of age, the number of RPE cells appeared normal in *Abca4*$^{-/-}$*Rdh8*$^{-/-}$ mice when compared with WT mice. The average number of RPE cells in *Abca4*$^{-/-}$*Rdh8*$^{-/-}$ mice per central portion of the imaging frame was 35.8 ± 2.8 compared with 32.2 ± 4.3 in WT mice. At 6 months of age, these average quantities for *Abca4*$^{-/-}$*Rdh8*$^{-/-}$ and WT mice were 33.6 ± 2.7 and 29.4 ± 3.4. These differences in RPE cell numbers were statistically insignificant. Unfortunately, the RPE cells could not be counted accurately in TPM images from *Mertk*$^{-/-}$*Abca4*$^{-/-}$*Rdh8*$^{-/-}$ and *Mertk*$^{-/-}$ mice because the RPE cell borders were obscured by fluorescence from the underlying layer of dying photoreceptors in 1-month-old mice and by a large quantity of fluorescent granules in 6-month-old animals. However, we did observe large areas devoid of fluorescence, indicative of RPE atrophy in both genotypes at 6 months of age.

TPM imaging of 1-month-old mice with 730 nm excitation light revealed an increased number of fluorescent deposits in the RPE cells of *Mertk*$^{-/-}$ and *Mertk*$^{-/-}$*Abca4*$^{-/-}$*Rdh8*$^{-/-}$ mice compared with WT and *Abca4*$^{-/-}$*Rdh8*$^{-/-}$ mice, suggesting a dominant *Mertk*$^{-/-}$ phenotype at this age (Fig. 4*A, top panel*). To determine the contribution of condensation products to this fluorescence, we then used TPM imaging with 850 nm excitation light. This analysis revealed increased total fluorescent signals in *Mertk*$^{-/-}$, *Mertk*$^{-/-}$*Abca4*$^{-/-}$*Rdh8*$^{-/-}$, and *Abca4*$^{-/-}$*Rdh8*$^{-/-}$ mice compared with WT mice, as well as focal spots with increased fluorescence in *Mertk*$^{-/-}$ and *Mertk*$^{-/-}$*Abca4*$^{-/-}$*Rdh8*$^{-/-}$ mice not seen in *Abca4*$^{-/-}$*Rdh8*$^{-/-}$ and WT mice. These data suggest accumulation of retinal condensation products by mice with a *Mertk*$^{-/-}$ background. The observation of fluorescence in the RPE nuclei at 730 nm excitation light with more pronounced fluorescence in the nuclei at 850 nm was indicative of fluorescence from the underlying layer of dying photoreceptors, as shown in more detail in supplemental movie 1 of the 3D reconstruction of the RPE-retina interface in *Mertk*$^{-/-}$ mice.

Enlarged fluorescent granules varying in size from 2 to 25 μm were detected in the RPE of *Mertk*$^{-/-}$ and *Mertk*$^{-/-}$*Abca4*$^{-/-}$*Rdh8*$^{-/-}$ mice at 6 months of age as compared with 1-month-old animals. Such granules were absent in mice with other backgrounds (Fig. 4*A, bottom panel*). Interestingly, these fluorescent granules were visible after excitation with both 730 and

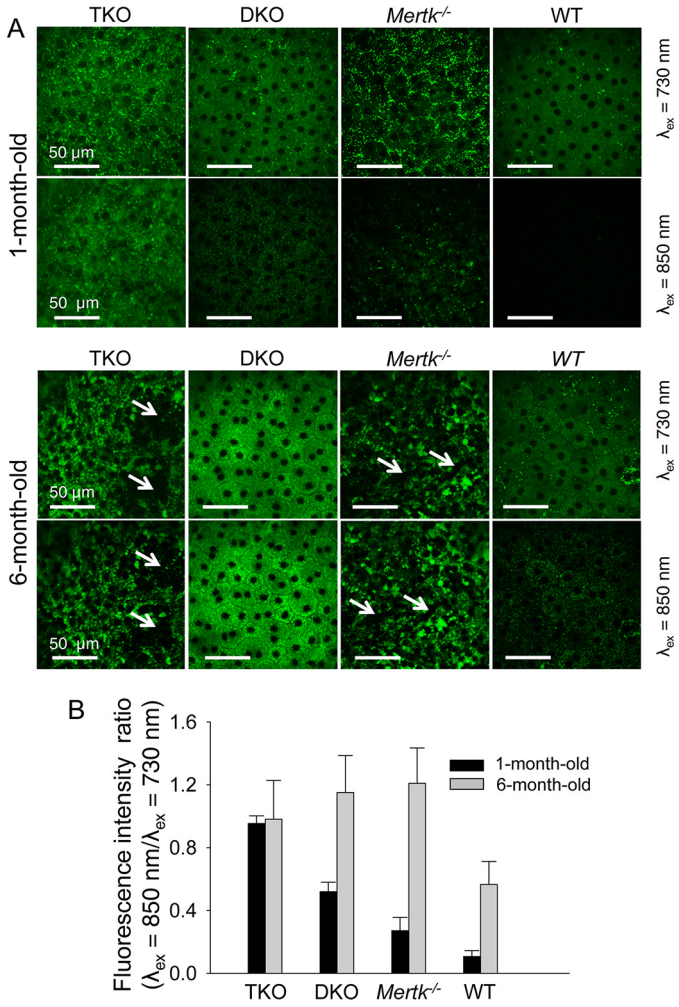

FIGURE 4. **Changes in mouse RPE with age.** *A,* TPM images of the RPE are shown in 1- and 6-month-old *Mertk*$^{-/-}$*Abca4*$^{-/-}$*Rdh8*$^{-/-}$ (TKO), *Abca4*$^{-/-}$*Rdh8*$^{-/-}$ (DKO), *Mertk*$^{-/-}$ and WT mice. Images display the superior portion of the retina 0.2 to 0.5 mm away from the optic nerve. In each panel, the *upper row images* were obtained with 730 nm excitation light and *lower row images* with 850 nm light. *Scale bars* indicate 50 μm. At 1 month of age, fluorescent particles located next to cell membranes responding to λ_{ex} = 730 nm but not λ_{ex} = 850 nm light (retinosomes) were present in all four mouse models. Additionally, all mice exhibited a continuous sheet of RPE cells. We counted on average 35.8 RPE cells per circular area with a diameter of 155 μm in DKO and an average of 32.2 cells in WT (S.D. were 2.8 and 4.3, respectively). At 6 months of age the average numbers of RPE cells per circular area with a diameter of 155 μm were 33.6 in DKO and 29.4 in WT mice (S.D. were 2.7 and 3.4, respectively). Precise counts of RPE cells in TKO and *Mertk*$^{-/-}$ mice were not feasible because RPE cell borders were shadowed by fluorescence from the photoreceptor layer at 1 month of age, and fluorescent granules with sizes varying from 2 to 25 μm and responding to both 730 and 850 nm excitation light were present at 6 months of age. Moreover, at the latter age, areas larger than 50 μm devoid of fluorescence (indicated with *white arrows*) were noted in the RPE of both TKO and *Mertk*$^{-/-}$ mice. *B,* differences in the contribution of fluorophores responding to 730 and 850 nm light among mice with different genetic backgrounds were quantified as ratios of fluorescence excited with 850 nm light to that excited with 730 nm light. *Bars* indicate S.D. $n \geq 3$ animals.

850 nm excitation light, indicating that they contain all-*trans*-retinal condensation products (17, 24). In contrast, increased but uniform background fluorescence was seen in 6-month-old *Abca4*$^{-/-}$*Rdh8*$^{-/-}$ mice as compared with 1-month-old mice. We then calculated the fluorescent intensity ratios (λ_{ex} = 850/730 nm), indicative of toxic condensation product accumulation (Fig. 4*B*) (24). At 1 month of age, *Mertk*$^{-/-}$*Abca4*$^{-/-}$*Rdh8*$^{-/-}$ mice displayed the highest fluorescent intensity ratio followed in order by *Abca4*$^{-/-}$*Rdh8*$^{-/-}$, *Mertk*$^{-/-}$, and WT mice. At this age, the fluorescence intensity in *Mertk*$^{-/-}$*Abca4*$^{-/-}$*Rdh8*$^{-/-}$ mice at λ_{ex} = 850 nm/λ_{ex} = 730 nm was roughly the sum of fluorescence observed for *Mertk*$^{-/-}$ and *Abca4*$^{-/-}$*Rdh8*$^{-/-}$ mice. At 6 months of age the fluorescence ratios increased in all mice. These findings indicate that toxic condensation products accumulate in the RPE of mice of different genotypes as a function of age, including mice lacking Mertk.

Larger cellular-shaped fluorescent deposits also were evident in the subretinal space of *Mertk*$^{-/-}$*Abca4*$^{-/-}$*Rdh8*$^{-/-}$ mice. Increased fluorescent spots and larger-sized signals were detected as well in 2-month-old *Mertk*$^{-/-}$ mice but not in WT mice (supplemental movies 1 and 2). *Mertk*$^{-/-}$ mice with an albino background serve as models of retinitis pigmentosa (25, 26) and start to exhibit signs of retinal degeneration at the age of 1 month before developing severe photoreceptor degeneration by the age of 6 months (Fig. 5).

Elevated Retinoid Condensation Products Are Present in the RPE of Phagocytosis-deficient Mutant Mice—To complement observations from TPM imaging, A2E, a major fluorescent bisretinoid condensation product, was quantified in our different mouse models by HPLC combined with tandem mass spectrometry (MS). Samples extracted from the eyes of 6-month-old *Mertk*$^{-/-}$*Abca4*$^{-/-}$*Rdh8*$^{-/-}$ mice revealed a chromatographic peak that had the same elution time and UV-visible spectrum as the A2E synthetic standard (Fig. 6*A*). Moreover, MS spectrum averaged at the peak indicated a dominant parent ion at *m*/*z* 592.6 $[MH]^+$, which correlates with the monoisotopic molecular mass of protonated A2E (Fig. 6*A, inset*). Additionally, the fragmentation patterns derived from this ion were identical to those of synthetic A2E (Fig. 6*B*). In *Mertk*$^{-/-}$*Abca4*$^{-/-}$*Rdh8*$^{-/-}$ as well as *Mertk*$^{-/-}$ mice, accumulation of A2E reached a plateau at 3 and 2 months of age. In contrast, *Abca4*$^{-/-}$*Rdh8*$^{-/-}$ mice kept accumulating A2E between 1 and 6 months of age. As expected from TPM imaging, quantification studies demonstrated that *Mertk*$^{-/-}$*Abca4*$^{-/-}$*Rdh8*$^{-/-}$ and *Mertk*$^{-/-}$ mutant mice accumulated significantly more A2E than WT mice (Fig. 6*C*). To determine the site(s) of A2E deposition, we isolated the neural retinas from the eyes of 6-month-old *Mertk*$^{-/-}$*Abca4*$^{-/-}$*Rdh8*$^{-/-}$ mice and performed an A2E analysis on the isolated retinas as well as the remaining eyecups containing the RPE. Both fractions had similar amounts of A2E (Fig. 6*D*). Thus, both the imaging and analytical methods demonstrated that elevated retinoid condensation products became incorporated in the RPE of mutant mice otherwise incapable of classical Mertk-dependent phagocytosis.

Primary RPE Cells Derived from Mertk$^{-/-}$ *Mice Have Compromised Phagocytotic Activity but Can Endocytose A2E*—To further examine whether fluorescent A2E-like condensation products observed in *Mertk*$^{-/-}$*Abca4*$^{-/-}$*Rdh8*$^{-/-}$ and *Mertk*$^{-/-}$ mice could result from RPE phagocytosis, primary RPE cells were isolated from *Mertk*$^{-/-}$ and WT mice to first assess their ability to phagocytize photoreceptor outer seg-

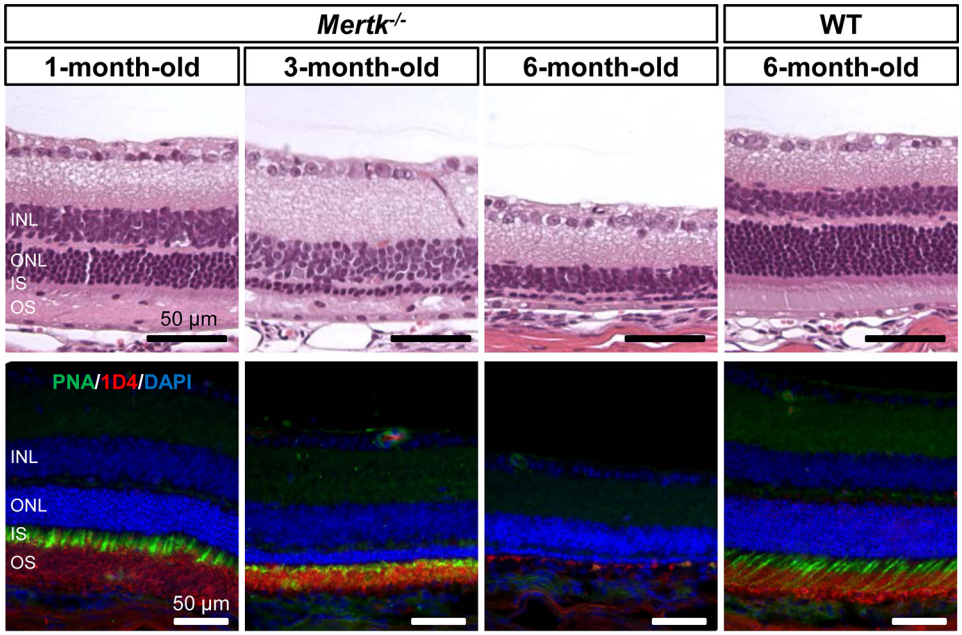

FIGURE 5. ***Mertk*$^{-/-}$ mice displayed progressive retinal degeneration.** Representative retinal morphology of 1-, 3-, and 6-month-old *Mertk*$^{-/-}$ mice and a 6-month-old WT control are shown. Retinal sections were stained with hematoxylin and eosin (*top panels*). *Scale bars,* 50 μm. Retinal sections were immunostained with PNA (*green*) for cone photoreceptor cells, anti-rhodopsin 1D4 (*red*) for rod outer segments, and DAPI (*blue*) for nuclei. *Scale bars,* 50 μm. *WT,* wild type; *INL,* inner nuclear layer; *ONL,* outer nuclear layer; *IS,* inner segment; *OS,* outer segment.

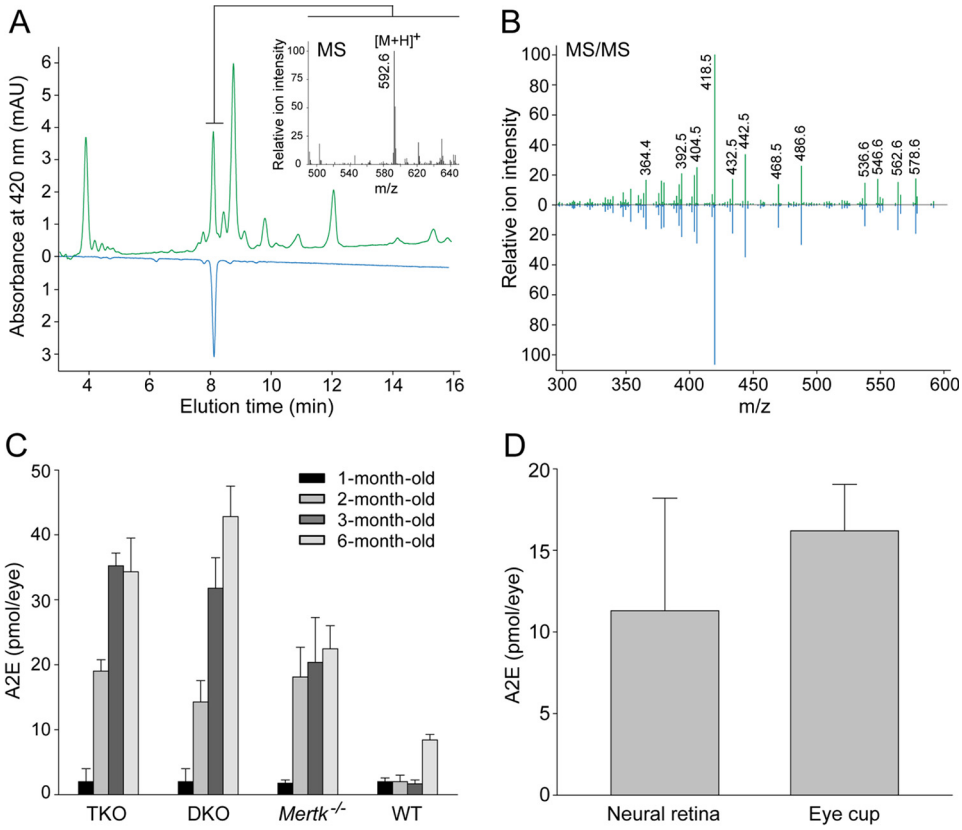

FIGURE 6. **Quantification of A2E in mouse eyes.** Analyses were done with a synthetic A2E standard and HPLC coupled to MS. *A,* chromatographic separation of organic compounds extracted from the eyes of 6-month-old *Mertk*$^{-/-}$*Abca4*$^{-/-}$*Rdh8*$^{-/-}$ mice (*green trace*). The peak corresponding to A2E was identified based on its retention time (*blue trace*), molecular mass (*inset*), and MS^2 fragmentation pattern (*B*), all of which were identical to an A2E synthetic standard. *C,* amounts of A2E in the eyes of *Mertk*$^{-/-}$*Abca4*$^{-/-}$*Rdh8*$^{-/-}$ (TKO), *Abca4*$^{-/-}$*Rdh8*$^{-/-}$ (DKO), *Mertk*$^{-/-}$, and WT mice at 1–3 and 6 months of age were quantified by HPLC. *Bars* indicate S.D. $n \geq 3$ animals. *D,* neural retina was isolated from the eyes of 6-month-old *Mertk*$^{-/-}$*Abca4*$^{-/-}$*Rdh8*$^{-/-}$ mice, and A2E quantification of the neural retina and the remaining eyecup was carried out. *Bars* indicate S.D. $n \geq 3$ animals. *mAU,* milliabsorbance unit.

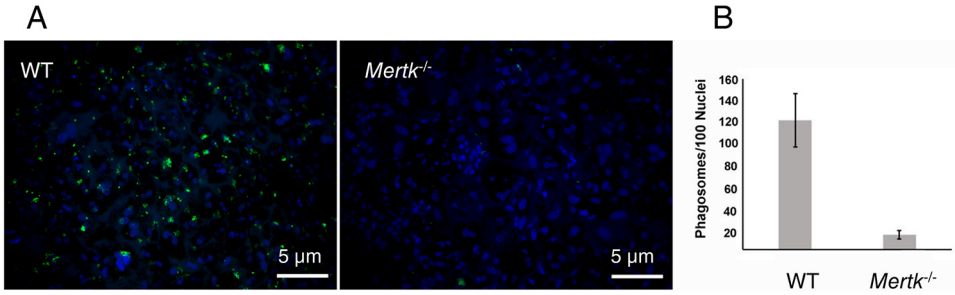

FIGURE 7. **Phagocytosis of fluorescein-labeled mouse rod outer segments (FITC-photoreceptor outer segments) by primary RPE cells.** The RPE from C57BL/6J and *Mertk*$^{-/-}$ mice was used to test its phagocytosis of photoreceptor outer segments. *A,* images of primary cultured RPE cells from C57BL/6J and *Mertk*$^{-/-}$ mice, which were challenged with FITC-outer segments *ex vivo*. The nuclei of challenged cells were stained with Hoechst 33342, mounted, and imaged with a Leica 600B fluorescence microscope. *B,* quantification of ingested particles was accomplished with ImageJ software and normalized to the number of nuclei present in each image ($n = 6–8$). *Scale bar,* 5 μm. Fluorescence representing phagocytized FITC-outer segments was observed in WT RPE cells, but only a residual amount was detected in the RPE from *Mertk*$^{-/-}$ mice.

ments. RPE cells were cultured for 1 week post-isolation and then were incubated with fluorescein-labeled photoreceptor outer segments for 1 h. In contrast to RPE cells isolated from WT mice that ingested the labeled outer segments, RPE cells from *Mertk*$^{-/-}$ mice exhibited little if any uptake of these segments (Fig. 7). For the 100 nuclei stained with Hoechst 33342, 121 ± 25.1 phagosomes were observed for WT RPE cells, but only 13.5 ± 4.2 phagosomes were associated with RPE cells from *Mertk*$^{-/-}$ mice. These data confirm that cultured primary RPE cells derived from *Mertk*$^{-/-}$ mice do indeed have compromised phagocytotic activity.

Because we confirmed that classic phagocytosis is absent in *Mertk*$^{-/-}$ mice, we employed a cell-based assay to test whether there is an alternative mechanism to transport A2E into the RPE. Isolated RPE cells from *Mertk*$^{-/-}$ and WT mice were incubated with A2E conjugated to 1% bovine serum albumin (BSA) and then analyzed for A2E accumulation by the same approach described above. Here, both RPE cells from *Mertk*$^{-/-}$ and WT mice accumulated similar levels of A2E (Fig. 8), indicating that transfer of A2E to RPE cells can occur independently of classic photoreceptor outer segment phagocytosis.

Activated Microglia Are Present in the Photoreceptor Cell Layers—We then attempted to identify a mechanism other than photoreceptor phagocytosis that could transfer A2E-like condensation products to the RPE. TPM revealed larger fluorescent cells in the photoreceptor layer of mutant mice (Fig. 9*A*), which displayed characteristics of activated microglia based on their size, fluorescent properties, and location (17). The TPM fluorescence emission spectrum from the microvilli region directly under the RPE was similar to that noted in the photoreceptor layer where activated microglia had infiltrated (Fig. 9*B*). This finding suggested that A2E-like condensation products had accumulated in microglia localized in both of these regions. Additionally, increased numbers of larger fluorescent spots indicative of activated microglia were noted in *Mertk*$^{-/-}$*Abca4*$^{-/-}$*Rdh8*$^{-/-}$ and *Mertk*$^{-/-}$ mice as compared with *Abca4*$^{-/-}$*Rdh8*$^{-/-}$ and WT mice (Fig. 9*C*). Moreover, additional experiments with bone marrow-derived macrophages demonstrated that these cells also could ingest A2E (Fig. 10, *A* and *B*). Finally, immunohistochemistry of retinal cells from *Mertk*$^{-/-}$*Abca4*$^{-/-}$*Rdh8*$^{-/-}$, *Abca4*$^{-/-}$*Rdh8*$^{-/-}$, and *Mertk*$^{-/-}$ mice further supported the presence of microglia capable of transferring A2E-like products from photoreceptor cells to the RPE (Fig. 10, *C* and *D*).

Discussion

In 1977, Edwards and Szamier (31) reported that the RPE in the Royal College of Surgeons (RCS) rat does not phagocytize photoreceptor outer segments. This observation was confirmed by Chaitin and Hall (57) who demonstrated that <10% of phagocytosis occurred in these rat RPE cells. Receptor tyrosine kinase Mertk (27) as well as a mutation in the human orthologue that causes retinitis pigmentosa (8) were identified as causative genes for this phagocytosis defective process. This contention was supported by mice with a disrupted *Mertk* gene, which display a phenotype similar to RCS rats (25). In this study, we used *Mertk*$^{-/-}$ mice in combination with *Abca4*$^{-/-}$*Rdh8*$^{-/-}$ mice to investigate the transfer of toxic retinoid condensation products that accumulate in the RPE. In juvenile animals, we found that higher quantities of fluorescent structures (retinosomes) were visible in *Mertk*$^{-/-}$*Abca4*$^{-/-}$*Rdh8*$^{-/-}$ and *Mertk*$^{-/-}$ mice than in *Abca4*$^{-/-}$*Rdh8*$^{-/-}$ and WT mice (17). Moreover, condensation fluorescent products also were present in *Mertk*$^{-/-}$*Abca4*$^{-/-}$*Rdh8*$^{-/-}$, *Abca4*$^{-/-}$*Rdh8*$^{-/-}$, and *Mertk*$^{-/-}$ mice. These fluorescent particles were uniformly distributed throughout the RPE cells of *Abca4*$^{-/-}$*Rdh8*$^{-/-}$ mice. In *Mertk*$^{-/-}$*Abca4*$^{-/-}$*Rdh8*$^{-/-}$ mice even at 1 month of age, the retina was already highly impacted by both massively dying photoreceptor cells and blockage of all-*trans*-retinal clearance; and *Mertk*$^{-/-}$*Abca4*$^{-/-}$*Rdh8*$^{-/-}$ mice exhibited fluorescence in their nuclei, indicative of dying photoreceptor cells (supplemental movie 2). The same was true for *Mertk*$^{-/-}$ mice but to a lesser degree. At an older age (6 months), (i) increased RPE fluorescence was observed in all animals with genetically altered backgrounds, with such fluorescence most pronounced in *Abca4*$^{-/-}$*Rdh8*$^{-/-}$, *Mertk*$^{-/-}$, and *Mertk*$^{-/-}$*Abca4*$^{-/-}$*Rdh8*$^{-/-}$ mice, and (ii) RPE cell structures were well preserved in both *Abca4*$^{-/-}$*Rdh8*$^{-/-}$ and WT mice. However, in *Mertk*$^{-/-}$*Abca4*$^{-/-}$*Rdh8*$^{-/-}$ or *Mertk*$^{-/-}$ mice, RPE cells were obstructed by fluorescence from the underlying layer of dying photoreceptor cells at 1 month of age and by large quantities of fluorescent granules or areas lacking fluorescence, extending by more than 50 μm, at 6 months of age.

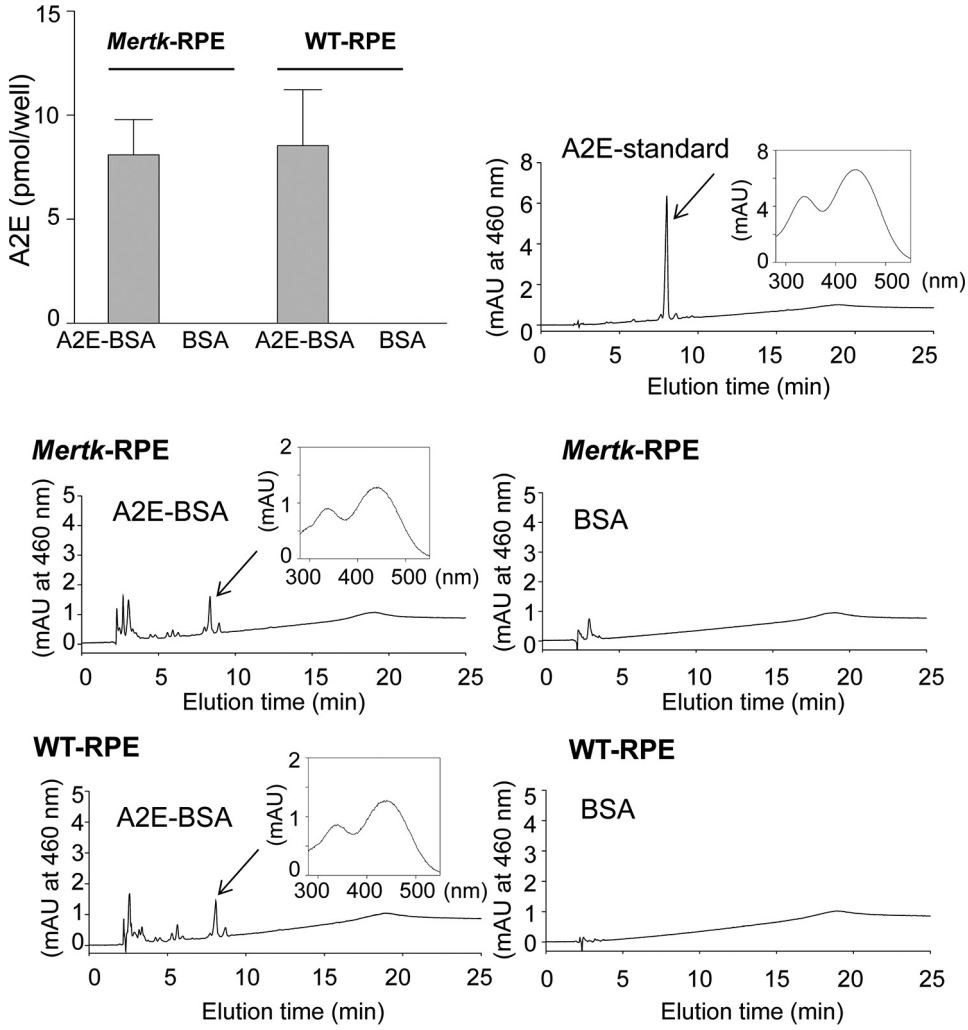

FIGURE 8. **A2E quantification in isolated primary RPE cells after incubation with A2E.** RPE cells, isolated from 12-day-old *Mertk*$^{-/-}$ and WT mice, were seeded onto 6.5-mm Transwell inserts that were co-incubated for 1 week with 40 μM A2E conjugated to bovine serum albumin (*BSA*). Equivalent amounts of 1% BSA alone were incubated with RPE cells as a control. A2E was then quantified in these differentially treated cells. HPLCs are shown, each with an *inset* of the spectrum of the peak depicted with an *arrow*. *Bars* indicate S.D. $n \geq 3$ animals. *mAU,* milliabsorbance unit.

Mertk$^{-/-}$ and *Mertk*$^{-/-}$*Abca4*$^{-/-}$*Rdh8*$^{-/-}$ mice accumulated A2E in the retina and RPE as determined by both TPM and quantitative analyses. Initially, these results were obtained in 1-month-old mice demonstrating either lower (*Mertk*$^{-/-}$) or higher (*Mertk*$^{-/-}$*Abca4*$^{-/-}$*Rdh8*$^{-/-}$) A2E accumulation. This difference had diminished in mice at 6 months of age, suggesting a maximal capacity of the retina/RPE to accumulate these retinoid by-products.

These findings support one of two possible mechanisms responsible for the accumulation of A2E. (i) A2E is transported independently of phagocytosis as part of a separate process that transfers hydrophobic substances such as docosahexaenoic acid (DHA) and retinoids between the retina and RPE. (ii) A2E is formed independently in both the retina and RPE. We favor the first option because little or no A2E accumulated in the retinas of *Rpe65*$^{-/-}$ mice lacking a visual cycle (28). In such mice, there is no flux of retinoids because fatty acid retinyl esters cannot be converted to 11-*cis*-retinal to regenerate rhodopsin. Moreover, *Cralbp*$^{-/-}$ mice, which possess active retinoid cycles, albeit with significantly reduced rates, failed to show elevated levels of retinal fluorescence (29). Also, isomerization occurs on demand, thus limiting the amount of 11-*cis*-retinal in the RPE (30).

The RPE supports vision in several ways, including phagocytizing the distal portions of photoreceptor outer segments (5). Phagocytosis is essential for the maintenance of vision as mutations affecting proteins required for this process lead to retinal degeneration in mammals (8, 9, 25, 31). Moreover, the RPE-photoreceptor outer segment interface is a site of reticular pseudo-drusen formation, accumulation of which directly correlates with the progression to AMD (32). In addition to conventional phagocytosis, there are other processes that contribute to the recycling of unsaturated lipids and retinoids critical to retinal health. Thus, a second transport system has been recognized but not described in detail. Key observations supporting such a second process include the following: (i) phagocytized DHA-containing lipids are recycled back to photoreceptors from the RPE in a process of rod/cone cell renewal that counters phagocytosis; (ii) 11-*cis*-retinoids are recycled effectively from phagosomes within RPE to photoreceptors; (iii) retinoids shuttle efficiently between the RPE and photoreceptor outer segments; (iv) mice deficient in

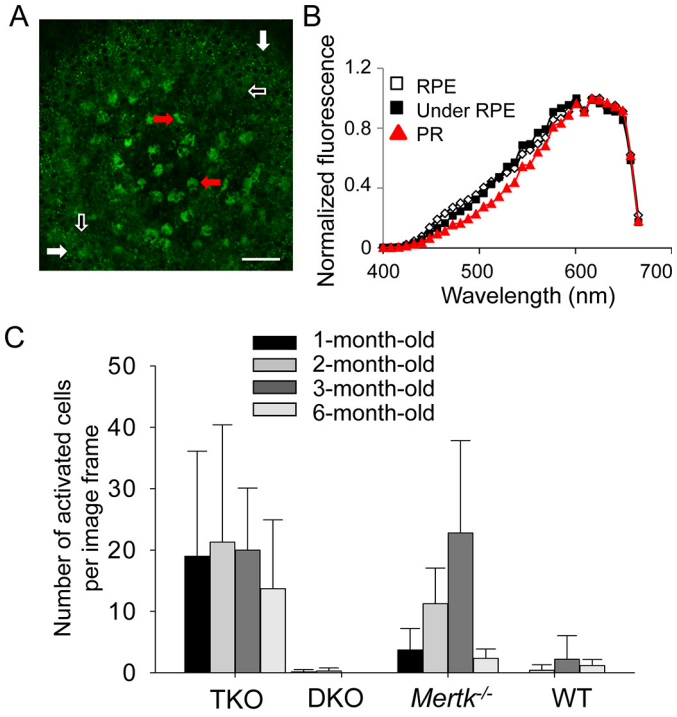

FIGURE 9. ***Mertk*$^{-/-}$ mice show increased quantities of activated microglia cells.** Activated microglia represent part of the retinal pathology noted in *Mertk*$^{-/-}$ mice. *A,* large field TPM image of the RPE and photoreceptor space in the eye of a 2-month-old *Mertk*$^{-/-}$*Abca4*$^{-/-}$*Rdh8*$^{-/-}$ (TKO) mouse. The eye curvature brings the RPE (*white arrows*) into a focus at the periphery of this image, with the photoreceptor space at the center. Activated cells are indicated with *red arrows*. The space directly under RPE is marked with *white-outlined black arrows*. *Scale bar,* 50 μm. *B,* TPM fluorescence emission spectra (with excitation at 730 nm) from the RPE, the space directly under the RPE, and from the photoreceptor space with activated microglial cells (PR) in a 2-month-old TKO mouse eye. *C,* quantities of activated microglial cells under the RPE and in the photoreceptor space (corresponding to the subretinal space) of TKO, *Abca4*$^{-/-}$*Rdh8*$^{-/-}$ (DKO), *Mertk*$^{-/-}$, and WT mice at the indicated ages are shown. *Bars* indicate S.D. of the means. $n \geq 3$ mice.

Mertk can still transfer bis-retinoids between these two cellular compartments; and (v) an array of nutrients must be continuously transferred through the RPE to photoreceptors. These considerations raise the intriguing question of how such non-phagocytic processes are regulated, and whether they could be enhanced to clear the inter-photoreceptor space of debris and thereby sustain the health of the RPE and photoreceptors.

Alternatively, tyrosine-protein kinase receptor TYRO3 and tyrosine-protein kinase receptor AXL could be involved in a phagocytosis-like transport process in the absence of MERTK (33). Collectively, TYRO3, AXL, and MERTK constitute the TAM receptor subfamily involved in phagocytosis. MERTK is one of three genes that constitute the TAM receptor subfamily involved in phagocytosis by different tissues and respond to the growth arrest-specific protein 6 (Gas6) ligand (33). Highly conserved AXL is involved in cell proliferation and also cell aggregation. TYRO3-encoded protein was identified in controlling cell survival and proliferation, immunoregulation, and phagocytosis, as well as a cell entry for Ebola and Marburg viruses. We found that the AXL transcript was most highly enriched in primary RPE cells and present in both the rodent and human retina/eye (Table 1). The number of normalized fragments/kilobase of exon per million mapped reads for MERTK and TYRO3 was similar but less abundant than for AXL. TAM receptors form obligatory homo- or heterodimers, and although MERTK is essential for phagocytosis of photoreceptor outer segments, these other receptors could be involved in alternative forms of phagocytosis. These structurally similar receptors are highly expressed in the eye and more specifically in the RPE (Table 1) (34, 35). In macrophages, tyrosine phosphorylation of Mertk in response to apoptotic cells is attenuated by deletion of the *Axl* and *Tyro3* genes, suggesting that these receptors interact, possibly by forming heterodimers (36). Indeed, *Tyro3 w*as identified as a murine genetic suppressor of Mertk-associated photoreceptor degeneration (37).

Another mechanism of transferring material between photoreceptors and RPE could involve adiponectin receptor(s) (AdipoRs). AdipoR1 and AdipoR2 are involved in regulating glucose levels and fatty acid breakdown (38). AdipoR1 acts as a regulatory switch of DHA uptake, retention, and conservation/elongation in photoreceptors and the RPE (39). AdipoR1 also is predicted to contain seven transmembrane domains, but it is structurally and functionally distinct from G protein-coupled receptors (40). Disruption of the *AdipoR1* gene results in diminished cellular DHA and a decrease in very long chain polyunsaturated fatty acids within the eye (39). Photoreceptor cells also display marked morphological abnormalities along with severely attenuated electroretinograms. Thus, AdipoRs could contribute to the transfer of material between macrophages and the RPE.

Age-dependent A2E accumulation in the RPE is recognized as a marker for human Stargardt disease, AMD, and normal aging (41). Chronic exposure to A2E may induce endogenous stress that causes low grade inflammation as is observed in diabetes, atherosclerosis, and age-related neurodegenerative diseases (42). Two characteristic features of low grade retinal chronic inflammation are complement deposition at Bruch's membrane and an increased number of subretinal microglia/macrophages (43). Although studies suggest a beneficial effect of these subretinal immune cells in tissue homeostasis (43–45), detrimental roles of activated microglial cells have been documented in AMD patients (46) and various disease models (47, 48). In this study, invasion of microglia into the subretinal space was documented in mice with retinal degeneration caused by Mertk deficiency. Interestingly, these subretinal microglia exhibited A2E-like spectral features. Moreover, microglia from the bone marrow also internalized A2E. Our study indicates that macrophages can contribute to A2E accumulation in the subretinal space and that A2E-associated inflammation can induce retinal degeneration (Fig. 11).

Materials and Methods

Animals—Abca4$^{-/-}$*Rdh8*$^{-/-}$ mice were generated as described previously (19), and all mice were genotyped by well established methods with the following primers: *Abca4* WT, 5′-GCCCAGTGGTCGATCTGTCTAGC-3′ and 5′-CGGACACAAAGGCCGCTAGGACCACG-3′; *Abca4* mutant, 5′-CCACAGCACACATCAGCATTTCTCC-3′ and 5′-TGCGAGGCCAGAGGCCACTTGTGTAGC-3′; *Rdh8* WT, 5′-CTTCAAAGTCAGTGGTGACTGGG-3′ and 5′-GCTATCCAGCTGCGACAATTC-3′; and *Rdh8* mutant, 5′-TCCGC-

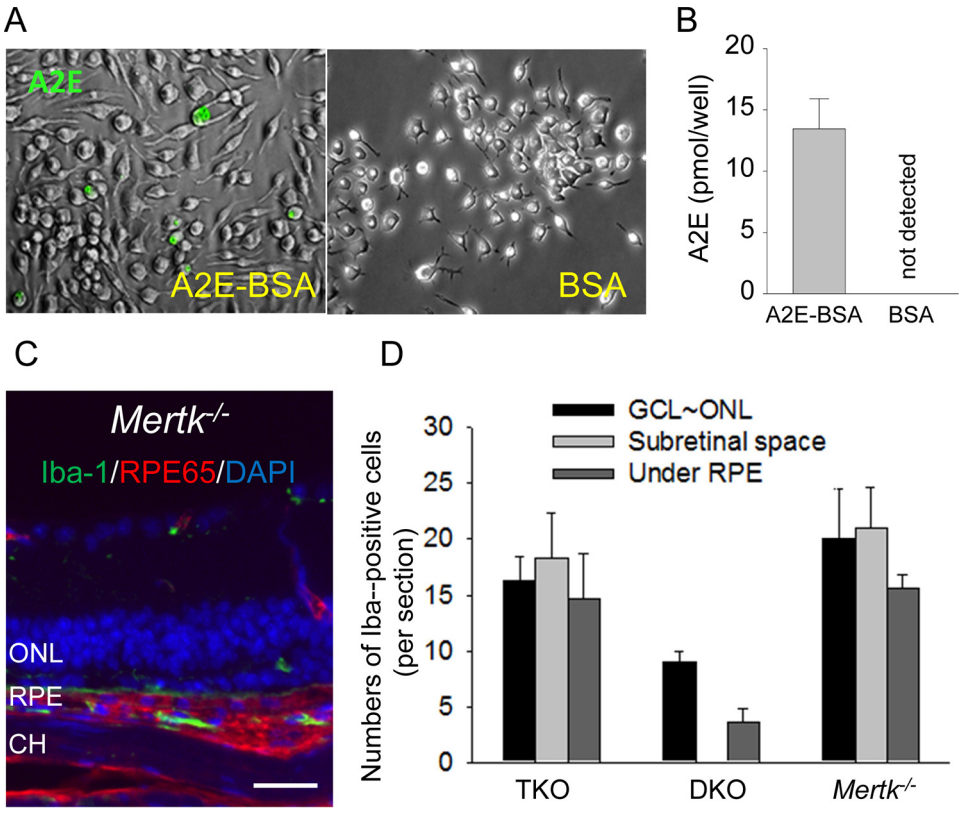

FIGURE 10. **Infiltration of microglia/macrophages into the subretinal space of *Mertk*$^{-/-}$ and *Mertk*$^{-/-}$*Abca4*$^{-/-}$*Rdh8*$^{-/-}$ mice.** *A* and *B,* bone marrow-derived macrophages seeded onto 6-well plates were co-incubated with either 40 μM A2E conjugated to bovine serum albumin (*BSA*) or BSA alone. *A,* representative bright field images (shown in *black* and *white*) are overlaid with autofluorescent images (shown in *green*), indicating A2E incorporated into these cells. *B,* A2E quantification by reverse-phase HPLC is presented. *Bars* indicate S.D. $n \geq 3$ animals or wells. *C* and *D,* retinal sections were immunostained with anti-Iba-1 antibody for microglia/macrophages (*green*), anti-RPE65 antibody for RPE cells (*red*), and DAPI for nuclei (*blue*). *C,* representative retinal section from a 6-month-old *Mertk*$^{-/-}$ mouse is presented. *Scale bars,* 20 μm. *D,* numbers of Iba-1-positive cells are shown. *GCL,* ganglion cell layer; *ONL,* outer nuclear layer; *CH,* choroid. *Bars* indicate S.D. $n \geq 3$ mice.

TABLE 1

Expression of TAM (*MERTK, TYRO3,* and *AXL*) receptor genes in rodents and human eyes and in primary RPE cell culture

Gene	Rat eye	Mouse eye	RPE cell culture	Human retina
AXL	14.0	11.4	125.6	2.8
MERTK	6.9	3.1	23.5	5.4
TYRO3	8.7	8.6	8.0	3.6

CTTGGAAACCTGAGCCAGAAG-3′ and 5′-TGCGAGGCCAGAGGCCACTTGTGTAGC-3′. *Mertk*$^{-/-}$ mice were purchased from The Jackson Laboratory (Bar Harbor, ME). *Mertk*$^{-/-}$*Abca4*$^{-/-}$*Rdh8*$^{-/-}$ mice, generated by cross-breeding *Mertk*$^{-/-}$ mice with *Abca4*$^{-/-}$*Rdh8*$^{-/-}$ mice, were subsequently genotyped (17). Genotyping of *Mertk*$^{-/-}$ mice was performed with the following primers: *Mertk* WT, 5′-GCTTTAGCCTCCCCAGTAGC-3′ and 5′-GGTCACATGCAAAGCAAATG-3′; *Mertk* mutant, 5′-CGTGGAGAAGGTAGTCGTACATCT-3′ and 5′-TTTGCCAAGTTCTAATTCCATC-3′.

For all genetic experiments, only mice with the Leu variation at amino acid 450 of RPE65 and free of the *Rd8* mutation were used. BALB/c mice from The Jackson Laboratory and their littermates were employed as WT controls. C57BL/6J mice also were purchased from The Jackson Laboratory. All mice were housed in the animal facility at the School of Medicine, Case Western Reserve University, where they were maintained on a normal mouse chow diet either under complete darkness or in a 12-h light (~10 lux)/12-h dark cyclic environment. An anesthetic mixture of 0.5% tropicamide and 0.5% phenylephrine hydrochloride (Midorin-P®) was obtained from Santen Pharmaceutical Co., Ltd. (Osaka, Japan); xylazine/AnaSed was from LLOYD, Inc. (Shenandoah, IA); and ketamine/Ketaset CIII was from Fort Dodge Animal Health (Fort Dodge, IA). Experimental manipulations of retinas and retinoid extractions were done in the dark under dim red light transmitted through a Kodak No. 1 safelight filter (transmittance >560 nm). All animal procedures and experiments were approved by the Case Western Reserve University Animal Care Committees and conformed to both the recommendations of the American Veterinary Medical Association Panel on Euthanasia and the Association for Research in Vision and Ophthalmology.

Clinical evaluation of the human patient from whom retinal tissue was obtained was carried out at the Cleveland Clinic Cole Eye Institute (Cleveland, OH). This research conformed to the tenets of the Declaration of Helsinki.

Chemicals—All-*trans*-retinal and phosphatidylethanolamine were purchased from Sigma and used for synthesis of A2E by a previously reported method (49).

Two-photon Excitation Analyses—TPM images and spectral characterization were carried out with a Leica TCS SP5 confocal MP system (Wetzlar, Germany) equipped with an upright DM6000 CFS stand. A tunable laser, Chameleon Vision-S (Coherent, Santa Clara, CA), was used that delivered 75-fs laser

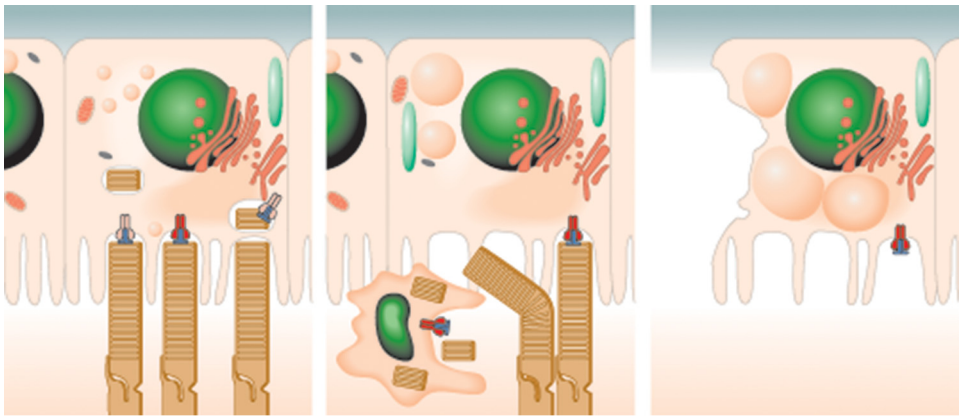

FIGURE 11. **Proposed sequence of pathological events in retinas of *Mertk*$^{-/-}$ *Abca4*$^{-/-}$*Rdh8*$^{-/-}$ mice.** In WT mice, A2E (and other retinal condensation products) in the form of small uniformly distributed granules slowly accumulates in the RPE as a result of photoreceptor outer segment phagocytosis by the RPE. In *Mertk*$^{-/-}$*Abca4*$^{-/-}$*Rdh8*$^{-/-}$ (TKO) mice, photoreceptor debris accumulates in the subretinal space and is taken up by infiltrating microglial cells. Microglial cells accumulate A2E. A2E material processed by microglia is absorbed by the RPE thereby contributing to large fluorescent granules shown. In old TKO mice besides large fluorescent granules (A2E), vacuoles and atrophies are also present in the RPE.

pulses at an 80-MHz pulse repetition frequency. Pulse duration at the sample was minimized by a dispersion pre-compensation system with settings that produced the largest two-photon excited fluorescence at a given laser power. Laser light was focused on the sample with a 20 × 1.0 NA water immersion Leica objective, and two-photon excited fluorescence was collected by the same lens. For imaging after filtration of excitation light by a Chroma ET680sp filter (Chroma Technology Corp., Bellows Falls, VT), the beam was directed to an HYD detector in a non-descanned manner. Emission spectra were obtained with a TCS SP5 spectrally sensitive HYD detector in a descanned configuration. Before imaging, laser power was measured at the sample plane and kept at 4–6 milliwatts with an electro-optic modulator. The same laser power and detector settings were used for each excitation wavelength when comparing fluorescence emitted in response to 730 nm excitation to that excited with 850 nm light. TPM was performed in intact enucleated mouse eyes, with the laser light and resulting fluorescence penetrating through the sclera. There was less than 15 min between eye enucleation and the start of TPM. Prior to enucleation, mice were anesthetized with an intraperitoneal injection of either anesthetic mixture 1 consisting of ketamine (16.5 mg/ml) and xylazine (1.65 mg/ml) diluted with water at a dose of 8–12 μl/g body weight or anesthetic mixture 2 consisting of ketamine (20 mg/ml) and xylazine (1.75 mg/ml) diluted with water at a dose of 4–5.2 μl/g body weight. Following anesthesia, mice were euthanized in compliance with the American Veterinary Medical Association (AVMA) Guidelines on Euthanasia, and approval by the Case Western Reserve University Institutional Animal Care and Use Committee. TPM 3D movies, reconstructions, and pixel gray values of raw retinal images were analyzed off-line with Leica LAS X software. SigmaPlot 11.0 software (Systat Software, Inc., San Jose, CA) was employed for statistical analyses of the obtained data.

RPE Phagocytosis Assays and A2E Incubation—Primary RPE cells were isolated from 12-day-old C57BL/6J or *Mertk*$^{-/-}$ pups (The Jackson Laboratory) using previously established protocols (50). Cells were seeded onto 6.5-mm Transwell inserts (0.4 μm pore, polyester; Sigma) at one eye per insert in a well with Dulbecco's modified Eagle's medium (DMEM, Invitrogen) supplemented with 1× nonessential amino acids (Sigma), 1× streptomycin/penicillin (Gibco, Life Technologies, Inc.), 10% fetal bovine serum (v/v) (Gibco, Life Technologies, Inc.) at 37 °C and 5% CO_2. Photoreceptor outer segments were isolated from mice, as described previously (51), and labeled with fluorescein isothiocyanate as per the manufacturer's instructions (Invitrogen Gibco, Life Technologies, Inc.). Labeled outer segments, diluted in growth media and added to the top chamber of a well containing RPE cells 1-week post-isolation, were incubated at 37 °C in 5% CO_2 for 1 h. Cells were washed three times with 1× Dulbecco's phosphate-buffered saline (DPBS) (Gibco, Life Technologies, Inc.), and externally bound FITC-outer segments were quenched by incubation with 0.4% trypan blue/DPBS (Gibco, Life Technologies, Inc.) for 10 min at room temperature. Cells were subsequently washed three times with 1× DPBS and placed in ice-cold methanol for 5 min before fixation with 4% paraformaldehyde/DPBS (Electron Microscopy Sciences; Hatfield, PA) for 10 min at room temperature. Nuclei were stained with Hoechst 33342 dye for 30 min at room temperature, and cells were washed three times with DPBS. Trans-well membranes were excised from the inserts and mounted on microscope slides with ProLong Gold Antifade reagent (Invitrogen Gibco, Life Technologies, Inc.). Mounted cells were imaged with a Leica 6000B fluorescence microscope (Wetzlar, Germany). Images were analyzed with ImageJ software, and ingested particles were counted and normalized to the number of nuclei present in the image.

For A2E studies, RPE cells were isolated as described previously (50) and seeded onto 6.5-mm Transwell inserts. After cells were allowed to attach for 48 h, the growth media were replaced with fresh media containing either 40 μM A2E conjugated to bovine serum albumin (BSA) or the same amount of 1% BSA (v/v) alone. A2E-BSA or BSA was replaced with fresh media every other day for 1 week. At the end of the experiment, cells were washed three times in DPBS and stored at −80 °C until analyzed.

A2E Quantification—After treatment with a Brinkmann Polytron homogenizer (Kinematica, Lucerne, Switzerland), endogenous A2E was extracted twice from either two frozen

eyes, two dissected neural retinas, two eyecups, or cultured cells in 1 ml of acetonitrile. Then upon evaporation of solvent, precipitates were dissolved in 150 μl of acetonitrile with 0.1% TFA (v/v), and filtered through a Teflon syringe filter. Samples (100 μl) were loaded on C18 columns (Phenomenex, Torrance, CA) and analyzed by reverse-phase HPLC with a mobile phase gradient of acetonitrile/H_2O from 100:0 to 80:20 with 0.1% TFA (v/v) for 20 min. Quantification of A2E was performed by comparison with known concentrations of a synthetic A2E standard.

Mass Spectrometry-based Analyses—Eye extracts from two eyes containing A2E (100 μl) were injected onto a Gemini 5-μm C18 110 Å (250 × 4.6 mm) column (Phenomenex, Torrance, CA). Retinoids then were separated with a gradient of isopropyl alcohol in acetonitrile (0–50%, v/v) over 15 min at a flow rate of 1 ml/min. Both solvents contained 0.1% formic acid (v/v). The eluent was directed into an LXQ linear ion trap mass spectrometer (Thermo Scientific, Waltham, MA) with an electrospray ionization probe that operated in a positive ionization mode. Tandem MS (MS/MS) spectra were collected by using collision-induced dissociation with the normalized collision energy set to 35 kV.

Retinoid Analyses—Retinoid extraction, derivation, and separation by HPLC were performed on samples extracted from eyes. Mice were euthanized by cervical dislocation, either immediately after light exposure or at indicated times after dark adaptation following such exposure, and eyes were removed with forceps. Eyes were deep frozen in dry ice or liquid nitrogen immediately after removal and stored at −80 °C until analysis. Frozen eyes were homogenized with a glass/glass homogenizer in 1 ml of retinoid analysis buffer (50 mM MOPS, 10 mM NH_4OH, and 50% ethanol in H_2O, pH 7.0). Retinoids were separated twice by centrifugation after adding 4 ml of hexane. Extracted retinoids in hexane were dried in a SpeedVac concentrator, suspended in 300 μl of hexane, and then separated by normal-phase HPLC (Ultrasphere-Si, 4.6 × 250 mm; Beckman Coulter, Brea, CA) in 10% ethyl acetate and 90% hexane (v/v) at a flow rate of 1.4 ml/min.

RNA-Seq, Read Mapping, and Determination of Reads per Kilobase per Million Reads (RPKM)—Rodent species (rat, *Rattus norvegicus* and mouse, *Mus musculus*) were euthanized by cervical dislocation, and eyes and retinal samples were dissected out and immediately placed in RNAlater stabilization reagent (Qiagen, Valencia, CA). The human retinal sample consisted of a tumor-free hemi-retina that was immediately placed in RNALater from a donor patient requiring enucleation for a large ocular melanoma. Library preparation for Illumina RNA-Seq (Illumina Inc., San Diego) was carried out as described previously (50). Libraries of *R. norvegicus, M. musculus*, and *Homo sapiens* were subjected to single-end sequencing with Illumina Genome Analyzer IIx or HiScan SQ. Data for *R. norvegicus, M. musculus*, and *H. sapiens* were processed and aligned with the University of California at Santa Cruz (UCSC; Santa Cruz, CA) rat (rn4), mouse (mm9), and human (hg19) genome assemblies and transcript annotations, respectively, using the Genomic Short-read Nucleotide Alignment Program (GSNAP), manual extraction of uniquely mapped reads, HTseq for raw read counts of genes, and manual calculation of RPKM (52) statistics by gene. The expression value for each transcript was calculated as RPKM (52) using a customized Perl script. The processed and raw fastq files for *M. musculus* were previously deposited in GEO (accession numbers GSE38359, GSE29752, and GSE48974), and the processed and raw fastq files for *R. norvegicus,* and *H. sapiens* are now deposited in the NCBI GEO database (accession numbers GSE84932 for *R. norvegicus* and GSE84930 for *H. sapiens*).

Histology and Immunohistochemistry—Mouse eyes were removed and fixed in 4% paraformaldehyde and 1% glutaraldehyde (v/v) for 48 h. Fixed specimens were embedded in paraffin, and 5-μm thick sections were cut and stained with hematoxylin and eosin (H&E). Immunohistochemistry was performed as described previously (53). Briefly, eyecups were dissected and fixed in 4% paraformaldehyde (v/v) overnight. Tissue was subjected to sucrose gradient centrifugation followed by embedment in a 20% sucrose/OCT (1:1) compound and freezing. Retinal sections (12 μm thick) were then prepared. Cryosections were incubated with one of the following primary antibodies: either rabbit anti-Iba-1 antibody (1:400; Wako); mouse anti-RPE65 antibody (1:200) (54); biotinylated peanut agglutinin (PNA) (1:400, Vector Laboratories); or anti-rhodopsin 1D4 antibody (0.1 mg/ml; 1:200) (a generous gift from Dr. R. S. Molday, University of British Columbia, Canada). Sections then were stained with either Alexa Fluor® 555 goat anti-rabbit IgG (H+L) (1:400, Invitrogen), Alexa Fluor® 488 goat anti-mouse IgG (H+L) (1:250, Invitrogen), Alexa Fluor® 488-conjugated streptavidin (1:500, Invitrogen), or Alexa Fluor® 555 goat anti-mouse IgG (H+L) (1:400, Invitrogen), respectively.

Electron Microscopy (EM)—Mouse eyecups were fixed by immersion in triple-aldehyde fixative for 48 h at room temperature as described previously (55). Triple-aldehyde fixative was prepared by mixing the same volume of fixative A (1 ml of 25% glutaraldehyde (EM Sciences), 1 ml of 20% paraformaldehyde (EM Sciences), 1 ml of 0.2 M HEPES buffer (EM Sciences), 1.95 ml of distilled water, 0.05 ml of Acrolein (EM Sciences), 2.5 μl of 1% $CaCl_2$, and 1% $MgCl_2$ with solution B (5% DMSO in H_2O)). After rinsing eyecups with distilled water, specimens were post-fixed in ferrocyanide-reduced osmium tetroxide, dehydrated in a graded series of ethanol, and then infiltrated and polymerized in epoxy resin, Poly/Bed 812. After polymerization, blocks were cut at 1 μm and stained with toluidine blue for light microscopy. After ultra-thin (90 nm) sectioning, cut sections were stained with uranyl acetate and Sato's triple lead stain, and examined with a Tecnai G2 Twin Spirit (FEI) equipped with a Gatan US4000 (4k×4k) ultra-high sensitivity CCD camera.

Isolation of Bone-derived Macrophages and Their Incubation with A2E—Bone marrow cells were harvested from the femurs of healthy 2-week-old C57BL/6J mice. Bones were cut at each end to expose the marrow and then centrifuged at 2000 × *g* for 30 s. Tissue from bones was treated with RBC lysis buffer (eBioscience, San Diego) to remove red blood cells. Bone marrow macrophages (BMM) then were suspended in growth medium (Dulbecco's modified Eagle's medium, 10% FBS, and 30% L929 conditioned medium) (56), plated in 6-well plates, and allowed to expand for 72 h. BMM were cultured with either BSA (0.1%) or A2E/BSA solution (40 μM A2E, 0.1% BSA) at 37 °C for 4 days. Cells were imaged by fluorescence microscopy with excitation/

emission at 495/519 nm wavelengths. Afterward, BMM cells were trypsinized, pelleted, and prepared for A2E quantification.

Quantification of Activated Microglia/Macrophages in the Retina—Microglia/macrophages (Iba-1-positive cells) were counted on cryostat sections of retinas from *Abca4*$^{-/-}$*Rdh8*$^{-/-}$ (DKO), *Mertk*$^{-/-}$, and *Mertk*$^{-/-}$*Abca4*$^{-/-}$*Rdh8*$^{-/-}$ (TKO) mice. Three areas were chosen for quantification of each section as follows: the region between the ganglion cell layer and the outer nuclear layer, the subretinal space, and the area under the RPE. Cell numbers represent the means ± S.D. of Iba-1-positive cells per retinal section.

Statistical Analyses—Data representing the means ± S.D. for the results of at least three independent experiments were compared by the one-way analysis of variance with a p value of <0.05 considered statistically significant.

Author Contributions—G. P., A. M., and K. P. conceived and designed the study. G. P., A. M., M. G., E. A., Z. D., L. P., and B. K. performed experiments and analyzed the data. G. P., A. M., and K. P. wrote the manuscript. All authors reviewed the results and approved the final version of the manuscript.

Acknowledgments—We thank Dr. Leslie T. Webster, Jr., and members of the Palczewski laboratory for valuable comments regarding this work. We also thank Dr. Debarshi Mustafi for the data provided in Table 1.

References

1. McBee, J. K., Palczewski, K., Baehr, W., and Pepperberg, D. R. (2001) Confronting complexity: the interlink of phototransduction and retinoid metabolism in the vertebrate retina. *Prog. Retin. Eye Res.* **20,** 469–529
2. Travis, G. H., Golczak, M., Moise, A. R., and Palczewski, K. (2007) Diseases caused by defects in the visual cycle: retinoids as potential therapeutic agents. *Annu. Rev. Pharmacol. Toxicol.* **47,** 469–512
3. Stone, J., Maslim, J., Valter-Kocsi, K., Mervin, K., Bowers, F., Chu, Y., Barnett, N., Provis, J., Lewis, G., Fisher, S. K., Bisti, S., Gargini, C., Cervetto, L., Merin, S., and Peér, J. (1999) Mechanisms of photoreceptor death and survival in mammalian retina. *Prog. Retin. Eye Res.* **18,** 689–735
4. Young, R. W., and Bok, D. (1969) Participation of the retinal pigment epithelium in the rod outer segment renewal process. *J. Cell Biol.* **42,** 392–403
5. Kevany, B. M., and Palczewski, K. (2010) Phagocytosis of retinal rod and cone photoreceptors. *Physiology* **25,** 8–15
6. Bok, D. (1993) The retinal pigment epithelium: a versatile partner in vision. *J. Cell Sci. Suppl.* **17,** 189–195
7. Kiser, P. D., Golczak, M., and Palczewski, K. (2014) Chemistry of the retinoid (visual) cycle. *Chem. Rev.* **114,** 194–232
8. Gal, A., Li, Y., Thompson, D. A., Weir, J., Orth, U., Jacobson, S. G., Apfelstedt-Sylla, E., and Vollrath, D. (2000) Mutations in MERTK, the human orthologue of the RCS rat retinal dystrophy gene, cause retinitis pigmentosa. *Nat. Genet.* **26,** 270–271
9. Vollrath, D., Feng, W., Duncan, J. L., Yasumura, D., D'Cruz, P. M., Chappelow, A., Matthes, M. T., Kay, M. A., and LaVail, M. M. (2001) Correction of the retinal dystrophy phenotype of the RCS rat by viral gene transfer of Mertk. *Proc. Natl. Acad. Sci. U.S.A.* **98,** 12584–12589
10. Molday, R. S. (2015) Insights into the molecular properties of ABCA4 and its role in the visual cycle and Stargardt disease. *Prog. Mol. Biol. Transl. Sci.* **134,** 415–431
11. Sparrow, J. R., Gregory-Roberts, E., Yamamoto, K., Blonska, A., Ghosh, S. K., Ueda, K., and Zhou, J. (2012) The bisretinoids of retinal pigment epithelium. *Prog. Retin. Eye Res.* **31,** 121–135
12. Holz, F. G., Bindewald-Wittich, A., Fleckenstein, M., Dreyhaupt, J., Scholl, H. P., Schmitz-Valckenberg, S., and FAM-Study Group. (2007) Progression of geographic atrophy and impact of fundus autofluorescence patterns in age-related macular degeneration. *Am. J. Ophthalmol.* **143,** 463–472
13. Gliem, M., Müller, P. L., Finger, R. P., McGuinness, M. B., Holz, F. G., and Charbel Issa, P. (2016) Quantitative fundus autofluorescence in early and intermediate age-related macular degeneration. *JAMA Ophthalmol.* **134,** 817–824
14. Batten, M. L., Imanishi, Y., Tu, D. C., Doan, T., Zhu, L., Pang, J., Glushakova, L., Moise, A. R., Baehr, W., Van Gelder, R. N., Hauswirth, W. W., Rieke, F., and Palczewski, K. (2005) Pharmacological and rAAV gene therapy rescue of visual functions in a blind mouse model of Leber congenital amaurosis. *PLoS Med.* **2,** e333
15. Van Hooser, J. P., Liang, Y., Maeda, T., Kuksa, V., Jang, G. F., He, Y. G., Rieke, F., Fong, H. K., Detwiler, P. B., and Palczewski, K. (2002) Recovery of visual functions in a mouse model of Leber congenital amaurosis. *J. Biol. Chem.* **277,** 19173–19182
16. Palczewska, G., Dong, Z., Golczak, M., Hunter, J. J., Williams, D. R., Alexander, N. S., and Palczewski, K. (2014) Noninvasive two-photon microscopy imaging of mouse retina and retinal pigment epithelium through the pupil of the eye. *Nat. Med.* **20,** 785–789
17. Maeda, A., Palczewska, G., Golczak, M., Kohno, H., Dong, Z., Maeda, T., and Palczewski, K. (2014) Two-photon microscopy reveals early rod photoreceptor cell damage in light-exposed mutant mice. *Proc. Natl. Acad. Sci. U.S.A.* **111,** E1428–E1437
18. Imanishi, Y., Batten, M. L., Piston, D. W., Baehr, W., and Palczewski, K. (2004) Noninvasive two-photon imaging reveals retinyl ester storage structures in the eye. *J. Cell Biol.* **164,** 373–383
19. Maeda, A., Maeda, T., Golczak, M., and Palczewski, K. (2008) Retinopathy in mice induced by disrupted all-*trans*-retinal clearance. *J. Biol. Chem.* **283,** 26684–26693
20. Kim, S. R., Nakanishi, K., Itagaki, Y., and Sparrow, J. R. (2006) Photooxidation of A2-PE, a photoreceptor outer segment fluorophore, and protection by lutein and zeaxanthin. *Exp. Eye Res.* **82,** 828–839
21. Ben-Shabat, S., Parish, C. A., Vollmer, H. R., Itagaki, Y., Fishkin, N., Nakanishi, K., and Sparrow, J. R. (2002) Biosynthetic studies of A2E, a major fluorophore of retinal pigment epithelial lipofuscin. *J. Biol. Chem.* **277,** 7183–7190
22. Imanishi, Y., Gerke, V., and Palczewski, K. (2004) Retinosomes: new insights into intracellular managing of hydrophobic substances in lipid bodies. *J. Cell Biol.* **166,** 447–453
23. Redmond, T. M., Yu, S., Lee, E., Bok, D., Hamasaki, D., Chen, N., Goletz, P., Ma, J. X., Crouch, R. K., and Pfeifer, K. (1998) Rpe65 is necessary for production of 11-cis-vitamin A in the retinal visual cycle. *Nat. Genet.* **20,** 344–351
24. Palczewska, G., Maeda, T., Imanishi, Y., Sun, W., Chen, Y., Williams, D. R., Piston, D. W., Maeda, A., and Palczewski, K. (2010) Noninvasive multiphoton fluorescence microscopy resolves retinol and retinal condensation products in mouse eyes. *Nat. Med.* **16,** 1444–1449
25. Duncan, J. L., LaVail, M. M., Yasumura, D., Matthes, M. T., Yang, H., Trautmann, N., Chappelow, A. V., Feng, W., Earp, H. S., Matsushima, G. K., and Vollrath, D. (2003) An RCS-like retinal dystrophy phenotype in mer knockout mice. *Invest. Ophthalmol. Vis. Sci.* **44,** 826–838
26. LaVail, M. M., Yasumura, D., Matthes, M. T., Yang, H., Hauswirth, W. W., Deng, W. T., and Vollrath, D. (2016) Gene therapy for MERTK-associated retinal degenerations. *Adv. Exp. Med. Biol.* **854,** 487–493
27. D'Cruz, P. M., Yasumura, D., Weir, J., Matthes, M. T., Abderrahim, H., LaVail, M. M., and Vollrath, D. (2000) Mutation of the receptor tyrosine kinase gene Mertk in the retinal dystrophic RCS rat. *Hum. Mol. Genet.* **9,** 645–651
28. Katz, M. L., and Redmond, T. M. (2001) Effect of Rpe65 knockout on accumulation of lipofuscin fluorophores in the retinal pigment epithelium. *Invest. Ophthalmol. Vis. Sci.* **42,** 3023–3030
29. Saari, J. C., Nawrot, M., Kennedy, B. N., Garwin, G. G., Hurley, J. B., Huang, J., Possin, D. E., and Crabb, J. W. (2001) Visual cycle impairment in cellular retinaldehyde binding protein (CRALBP) knockout mice results in delayed dark adaptation. *Neuron* **29,** 739–748
30. Stecher, H., Gelb, M. H., Saari, J. C., and Palczewski, K. (1999) Preferential release of 11-*cis*-retinol from retinal pigment epithelial cells in the pres-

ence of cellular retinaldehyde-binding protein. *J. Biol. Chem.* **274,** 8577–8585
31. Edwards, R. B., and Szamier, R. B. (1977) Defective phagocytosis of isolated rod outer segments by RCS rat retinal pigment epithelium in culture. *Science* **197,** 1001–1003
32. Zweifel, S. A., Spaide, R. F., Curcio, C. A., Malek, G., and Imamura, Y. (2010) Reticular pseudodrusen are subretinal drusenoid deposits. *Ophthalmology* **117,** 303–312
33. Lemke, G., and Rothlin, C. V. (2008) Immunobiology of the TAM receptors. *Nat. Rev. Immunol.* **8,** 327–336
34. Prasad, D., Rothlin, C. V., Burrola, P., Burstyn-Cohen, T., Lu, Q., Garcia de Frutos, P., and Lemke, G. (2006) TAM receptor function in the retinal pigment epithelium. *Mol. Cell. Neurosci.* **33,** 96–108
35. Lu, Q., Gore, M., Zhang, Q., Camenisch, T., Boast, S., Casagranda, F., Lai, C., Skinner, M. K., Klein, R., Matsushima, G. K., Earp, H. S., Goff, S. P., and Lemke, G. (1999) Tyro-3 family receptors are essential regulators of mammalian spermatogenesis. *Nature* **398,** 723–728
36. Seitz, H. M., Camenisch, T. D., Lemke, G., Earp, H. S., and Matsushima, G. K. (2007) Macrophages and dendritic cells use different Axl/Mertk/Tyro3 receptors in clearance of apoptotic cells. *J. Immunol.* **178,** 5635–5642
37. Vollrath, D., Yasumura, D., Benchorin, G., Matthes, M. T., Feng, W., Nguyen, N. M., Sedano, C. D., Calton, M. A., and LaVail, M. M. (2015) Tyro3 modulates Mertk-associated retinal degeneration. *PLoS Genet.* **11,** e1005723
38. Yamauchi, T., Kamon, J., Ito, Y., Tsuchida, A., Yokomizo, T., Kita, S., Sugiyama, T., Miyagishi, M., Hara, K., Tsunoda, M., Murakami, K., Ohteki, T., Uchida, S., Takekawa, S., Waki, H., *et al.* (2003) Cloning of adiponectin receptors that mediate antidiabetic metabolic effects. *Nature* **423,** 762–769
39. Rice, D. S., Calandria, J. M., Gordon, W. C., Jun, B., Zhou, Y., Gelfman, C. M., Li, S., Jin, M., Knott, E. J., Chang, B., Abuin, A., Issa, T., Potter, D., Platt, K. A., and Bazan, N. G. (2015) Adiponectin receptor 1 conserves docosahexaenoic acid and promotes photoreceptor cell survival. *Nat. Commun.* **6,** 6228
40. Tanabe, H., Fujii, Y., Okada-Iwabu, M., Iwabu, M., Nakamura, Y., Hosaka, T., Motoyama, K., Ikeda, M., Wakiyama, M., Terada, T., Ohsawa, N., Hato, M., Ogasawara, S., Hino, T., Murata, T., *et al.* (2015) Crystal structures of the human adiponectin receptors. *Nature* **520,** 312–316
41. Delori, F. C., Goger, D. G., and Dorey, C. K. (2001) Age-related accumulation and spatial distribution of lipofuscin in RPE of normal subjects. *Invest. Ophthalmol. Vis. Sci.* **42,** 1855–1866
42. Medzhitov, R. (2008) Origin and physiological roles of inflammation. *Nature* **454,** 428–435
43. Xu, H., Chen, M., and Forrester, J. V. (2009) Para-inflammation in the aging retina. *Prog. Retin. Eye Res.* **28,** 348–368
44. Bruban, J., Maoui, A., Chalour, N., An, N., Jonet, L., Feumi, C., Tréton, J., Sennlaub, F., Behar-Cohen, F., Mascarelli, F., and Dinet, V. (2011) CCR2/CCL2-mediated inflammation protects photoreceptor cells from amyloid-β-induced apoptosis. *Neurobiol. Dis.* **42,** 55–72
45. Ma, W., Zhao, L., Fontainhas, A. M., Fariss, R. N., and Wong, W. T. (2009) Microglia in the mouse retina alter the structure and function of retinal pigmented epithelial cells: a potential cellular interaction relevant to AMD. *PLoS ONE* **4,** e7945
46. Sennlaub, F., Auvynet, C., Calippe, B., Lavalette, S., Poupel, L., Hu, S. J., Dominguez, E., Camelo, S., Levy, O., Guyon, E., Saederup, N., Charo, I. F., Rooijen, N. V., Nandrot, E., Bourges, J. L., *et al.* (2013) CCR2(+) monocytes infiltrate atrophic lesions in age-related macular disease and mediate photoreceptor degeneration in experimental subretinal inflammation in Cx3cr1 deficient mice. *EMBO Mol. Med.* **5,** 1775–1793
47. Hu, S. J., Calippe, B., Lavalette, S., Roubeix, C., Montassar, F., Housset, M., Levy, O., Delarasse, C., Paques, M., Sahel, J. A., Sennlaub, F., and Guillonneau, X. (2015) Upregulation of P2RX7 in Cx3cr1-deficient mononuclear phagocytes leads to increased interleukin-1β secretion and photoreceptor neurodegeneration. *J. Neurosci.* **35,** 6987–6996
48. Kohno, H., Chen, Y., Kevany, B. M., Pearlman, E., Miyagi, M., Maeda, T., Palczewski, K., and Maeda, A. (2013) Photoreceptor proteins initiate microglial activation via Toll-like receptor 4 in retinal degeneration mediated by all-*trans*-retinal. *J. Biol. Chem.* **288,** 15326–15341
49. Parish, C. A., Hashimoto, M., Nakanishi, K., Dillon, J., and Sparrow, J. (1998) Isolation and one-step preparation of A2E and iso-A2E, fluorophores from human retinal pigment epithelium. *Proc. Natl. Acad. Sci. U.S.A.* **95,** 14609–14613
50. Mustafi, D., Kevany, B. M., Genoud, C., Okano, K., Cideciyan, A. V., Sumaroka, A., Roman, A. J., Jacobson, S. G., Engel, A., Adams, M. D., and Palczewski, K. (2011) Defective photoreceptor phagocytosis in a mouse model of enhanced S-cone syndrome causes progressive retinal degeneration. *FASEB J.* **25,** 3157–3176
51. Liang, Y., Fotiadis, D., Filipek, S., Saperstein, D. A., Palczewski, K., and Engel, A. (2003) Organization of the G protein-coupled receptors rhodopsin and opsin in native membranes. *J. Biol. Chem.* **278,** 21655–21662
52. Mortazavi, A., Williams, B. A., McCue, K., Schaeffer, L., and Wold, B. (2008) Mapping and quantifying mammalian transcriptomes by RNA-Seq. *Nat. Methods* **5,** 621–628
53. Maeda, A., Maeda, T., Imanishi, Y., Kuksa, V., Alekseev, A., Bronson, J. D., Zhang, H., Zhu, L., Sun, W., Saperstein, D. A., Rieke, F., Baehr, W., and Palczewski, K. (2005) Role of photoreceptor-specific retinol dehydrogenase in the retinoid cycle *in vivo*. *J. Biol. Chem.* **280,** 18822–18832
54. Golczak, M., Kiser, P. D., Lodowski, D. T., Maeda, A., and Palczewski, K. (2010) Importance of membrane structural integrity for RPE65 retinoid isomerization activity. *J. Biol. Chem.* **285,** 9667–9682
55. Fujioka, H., Tandler, B., Cohen, M., Koontz, D., and Hoppel, C. L. (2014) Multiple mitochondrial alterations in a case of myopathy. *Ultrastruct. Pathol.* **38,** 204–210
56. Johnson, A. C., Li, X., and Pearlman, E. (2008) MyD88 functions as a negative regulator of TLR3/TRIF-induced corneal inflammation by inhibiting activation of c-Jun N-terminal kinase. *J. Biol. Chem.* **283,** 3988–3996
57. Chaitin, M. H., and Hall, M. O. (1983) Defective ingestion of rod outer segments by cultured dystrophic rat pigment epithelial cells. *Invest. Ophthalmol. Vis. Sci.* **24,** 812–820